PHYSICAL REVIEW B **86**, 125448 (2012)

Coulomb drag in graphene–boron nitride heterostructures: Effect of virtual phonon exchange

Bruno Amorim,[1] Jürgen Schiefele,[2] Fernando Sols,[2] and Francisco Guinea[1]
[1]*Instituto de Ciencia de Materiales de Madrid, CSIC, Cantoblanco, E-28 049, Madrid, Spain*
[2]*Departamento de Física de Materiales, Universidad Complutense de Madrid, E-28 040, Madrid, Spain*

(Received 18 June 2012; revised manuscript received 22 August 2012; published 27 September 2012)

For a system of two spatially separated monoatomic graphene layers encapsulated in hexagonal boron nitride, we consider the drag effect between charge carriers in the Fermi liquid regime. Commonly, the phenomenon is described in terms of an interlayer Coulomb interaction. We show that if an additional electron–electron interaction via exchange of virtual substrate phonons is included in the model, the predicted drag resistivity is modified considerably at temperatures above 150 K. The anisotropic crystal structure of boron nitride, with strong intralayer and comparatively weak interlayer bonds, is found to play an important role in this effect.

DOI: 10.1103/PhysRevB.86.125448 PACS number(s): 72.80.Vp, 77.84.Bw

I. INTRODUCTION

If two systems containing mobile charge carriers are spatially separated such that direct charge transfer is not possible, but close enough to allow interaction between the carriers in different layers, the resulting momentum transfer will equalize the drift velocities in both systems. This frictional effect was experimentally observed between (quasi) two-dimensional electron gases in double quantum well structures.[1,2] In most of the theoretical work the interlayer interaction was attributed to Coulomb scattering, hence the effect now bears the name "Coulomb drag" (see Refs. 3–5).

Interest in the subject has been revived recently by the experimental progress which made it possible to prepare two-dimensional electron systems based on monolayer graphene. A considerable number of theoretical works[6–16] studied Coulomb drag between massless Dirac fermions, which effectively describe the charge carriers in graphene.[17] However, a quantitatively correct explanation of the experimental data is still lacking.[6,18–20]

In the typical experiment, Coulomb drag is studied by driving a constant current I_2 through one of the layers (the active one, labeled by the index $\lambda = 2$ in Fig. 1). If no current is allowed to flow in the other (passive, index 1) layer, a potential difference V_1 builds up there. In terms of these two quantities, the drag resistivity $\rho_D \equiv (W/L)V_1/I_2$ serves as a measure of the momentum transfer between the two layers, where W and L are, respectively, the width and the length of the layer. A theoretical expression for ρ_D in second order in the interlayer interaction can be derived either using Boltzmann's kinetic equation[4,10,11,21] or the Kubo formula.[5,9,11]

In the present work we focus on the interlayer interaction responsible for the drag effect in heterostructures composed of two graphene monolayers and hexagonal boron nitride (hBN), see Fig. 1. The large band gap insulator hBN has a layered structure composed of stacked hexagonal crystal planes. Recently the material received much attention as it allows the construction of graphene–hBN devices with, in comparison to the much used SiO_2 substrates, favorable high carrier mobilities.[22–25] In particular, the Manchester group reported the fabrication of devices where a few layer thin hBN crystal, obtained by exfoliation, is sandwiched between two monolayers of graphene.[26–28] If such a structure is used for a Coulomb drag experiment, the Dirac fermions in the active and passive layer can exchange momentum not only via Coulomb interaction but also by phonon exchange through the spacer medium. The effect of a combined Coulomb-phonon coupling on the drag resistivity has previously only been studied for quasi-two-dimensional electron gases in semiconductor systems.[29–34]

In the following we first investigate the effects of the anisotropy of hBN, where the bonds in between the graphene-like planes are much weaker than the in-plane bonds, on the electron–electron interaction via phonon exchange. We then show that the inclusion of phonon exchange into the description of Coulomb drag can significantly alter the temperature, density, and distance dependence of the predicted value for ρ_D at temperatures above 150 K.

II. INTERLAYER INTERACTION

A. Combined Coulomb–phonon mediated interaction

In a two-layer system as shown in Fig. 1, where the regions I, II, and III are filled with a homogeneous isotropic dielectric medium, the Fourier transform of the bare (unscreened) Coulomb potential between electrons in layers λ and λ' has the form

$$V^{(0)}_{\lambda\lambda'}(q) = \frac{1}{\epsilon_\infty}\frac{e^2}{2\epsilon_{\mathrm{vac}} q} e^{-qd(1-\delta_{\lambda\lambda'})}, \tag{1}$$

where $\mathbf{q} = (q_x, q_y)$, ϵ_{vac} denotes the dielectric constant of vacuum and ϵ_∞ accounts for the high frequency screening properties of the medium. Apart from this Coulomb interaction, the charge carriers in each graphene layer interact via a substrate phonon mediated interaction. The charge carriers from each layer couple to the long range electric fields generated by optically active phonon modes in the surrounding material via Fröhlich coupling.[35–37] This remote interaction between carriers in graphene and optical phonon modes in a substrate medium was found to influence the electrical conductivity of graphene on a dielectric substrate.[24,38,39]

In Appendix A we show that in an isotropic medium the combined interaction between electrons in layers λ and λ' via the effects of a static Coulomb potential and virtual substrate phonon exchange is of the form of Eq. (1), with ϵ_∞ replaced by the frequency dependent dielectric function $\epsilon(\omega)$ of the substrate material [see Eq. (A7)].

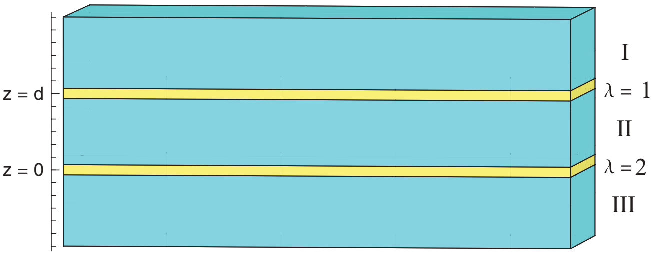

FIG. 1. (Color online) A sketch of the double layer system under consideration. The two monoatomic graphene layers (yellow) with charge carrier concentration n_1, n_2 are placed at $z = 0$ and $z = d$ and labeled by the layer index $\lambda = 1,2$, respectively. The surrounding space (regions I, II, and III) is filled with the insulating material boron nitride with hexagonal structure (hBN).

In the following we specialize to the anisotropic spacer material hBN. From its three acoustic and nine optical phonon bands, only those that (via dipole oscillations) create long range electric fields couple to the graphene electrons.[40] Given the layered uniaxial crystal structure of hBN, these (infrared active) optical modes are described by a dielectric tensor of the form[41]

$$\boldsymbol{\epsilon}(\omega) = \mathrm{diag}[\epsilon_\perp(\omega),\epsilon_\perp(\omega),\epsilon_\parallel(\omega)]. \tag{2}$$

The resonance frequencies $\omega_{\rm TO}^{\parallel}$ and $\omega_{\rm TO}^{\perp}$ of the two retarded[42] dielectric functions

$$\epsilon_{\perp,\parallel}(\omega) = \epsilon_\infty^{\perp,\parallel} + f_{\perp,\parallel}\frac{(\omega_{\rm TO}^{\perp,\parallel})^2}{(\omega_{\rm TO}^{\perp,\parallel})^2 - \omega^2 - i\omega\gamma_{\perp,\parallel}} \tag{3}$$

are the phonon frequencies at the Γ point for transverse intraplane shear modes with displacements parallel and perpendicular to the c axis of the crystal (aligned with the z direction in Fig. 1), respectively. We make the usual approximation of dispersionless optical phonon bands.[29,35,43] The values for the high frequency dielectric constants ϵ_∞, the oscillator strengths f (related to the static ϵ_0 and high frequency dielectric constants $f = \epsilon_0 - \epsilon_\infty$), $\omega_{\rm TO}$, and the damping factors γ taken from Ref. 44 are listed in Table I.

To obtain the combined Coulomb-phonon interaction $U^{(0)}_{\lambda\lambda'}$ in the anisotropic medium, we solve Poisson's equation

$$-\nabla \cdot (\boldsymbol{\epsilon} \cdot \nabla\phi) = \rho_{\rm free}/\epsilon_{\rm vac}$$

with $\rho_{\rm free}$ being the free charge density of a point charge $-e$ at the origin. With Eq. (2), Poisson's equation becomes

$$-\frac{\partial}{\partial z}\left[\epsilon_\parallel \frac{\partial}{\partial z}\phi(\boldsymbol{q},z)\right] + q^2\epsilon_\perp\phi(\boldsymbol{q},z) = -\frac{e}{\epsilon_{\rm vac}}\delta(z),$$

and as $U^{(0)}_{12} = -e\phi(q,d)$ and $U^{(0)}_{11} = U^{(0)}_{22} = -e\phi(q,0)$ we get

$$U^{(0)}_{\lambda\lambda'}(q,\omega) = \frac{e^2}{2\epsilon_{\rm vac}\epsilon_\parallel(\omega)q}\sqrt{\frac{\epsilon_\parallel(\omega)}{\epsilon_\perp(\omega)}} \times \exp\left[-qd(1-\delta_{\lambda\lambda'})\sqrt{\frac{\epsilon_\perp(\omega)}{\epsilon_\parallel(\omega)}}\right]. \tag{4}$$

A generalization of this result to structures where the regions I, II, and III (see Fig. 1) are filled with different insulating materials (or air) is straightforward; $U^{(0)}_{11}$ then involves different dielectric functions than $U^{(0)}_{22}$.

TABLE I. Parameters for the dielectric function of hBN [see Eq. (3)] taken from Ref. 44.[a]

	$\epsilon_\perp$	$\epsilon_\parallel$
ϵ_∞	4.95	4.10
f	1.868	0.532
γ	3.61 meV	0.995 meV
$\omega_{\rm TO}$	170 meV	97.4 meV

[a] The experimental data in Ref. 44 exhibits two resonances, a strong and a weaker one, for each direction of the polarization of incident light. The weaker ones are attributed to misorientation of the polycrystalline samples.

B. RPA screened interlayer interaction

To take into account the screening properties of the conduction electrons in the graphene layers themselves, we employ the standard procedure of solving the Dyson equation for the two-layer system within the random phase approximation (RPA) (see Ref. 5). This finally yields the dressed interlayer interaction

$$U_{12}(q,\omega) = \frac{U^{(0)}_{12}(q,\omega)}{\epsilon_{\rm RPA}(q,\omega)}. \tag{5}$$

The total screening function for the coupled electron-phonon system given by (see Ref. 31 and Appendix B)

$$\epsilon_{\rm RPA} = \left(1 - U^{(0)}_{11}\chi_1\right)\left(1 - U^{(0)}_{22}\chi_2\right) - U^{(0)}_{12}U^{(0)}_{21}\chi_1\chi_2, \tag{6}$$

where $\chi_{1,2}$ denotes the (frequency and momentum dependent) polarizability of the graphene layers.[45]

Figure 2 shows a density plot of $|\epsilon_{\rm RPA}(q,\omega)|$, using dimensionless units $x = q/k_F$ and $y = \omega/(v_F k_F)$, where k_F is the Fermi momentum. The horizontal dashed green lines mark the transverse and longitudinal frequencies of the infrared active modes in hBN, connected by the Lyddane-Sachs-Teller relation[46] $\omega_{\rm LO}^2/\omega_{\rm TO}^2 = \epsilon_0/\epsilon_\infty$. For small damping $\gamma \ll \omega_{\rm TO}$, the real parts of $\epsilon_{\perp,\parallel}(\omega)$ are close to a pole at $\omega_{\rm TO}^{\perp,\parallel}$ and close to zero at $\omega_{\rm LO}^{\perp,\parallel}$, respectively. Near these frequencies, the absolute value of the total screening function $\epsilon_{\rm RPA}$ likewise shows an abrupt change from high values (light colors) to almost zero (dark colors). In regions where $|\epsilon_{\rm RPA}|$ is small, the red lines $\mathrm{Re}\,\epsilon_{\rm RPA} = 0$ show the coupled plasmon-phonon dispersion relation of the two-layer system.

III. RESULTS FOR THE DRAG RESISTIVITY

In the following we assume for the sake of simplicity the same positive carrier density n (corresponding to electron doping) in both layers, such that $E_F \gg k_B T$. In particular, we do not address the recently reported drag at charge neutrality point,[20] which was attributed either to contributions from higher order perturbation theory[15] or to correlated density inhomogenities in the graphene layers.[16,20]

The drag resistivity then assumes a negative value,[18] and the first nonvanishing contribution to ρ_D obtained in perturbation

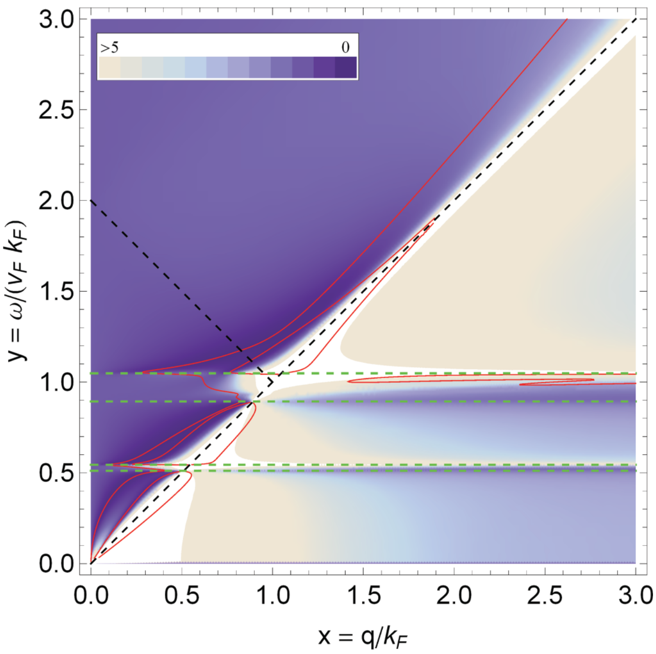

FIG. 2. (Color online) Absolute value of the total screening function $\epsilon_{\rm RPA}$ Eq. (6), with $n_1 = n_2 = 0.02$ nm^{-2} and $d = 8$ nm. Vertical green lines show the optical resonance frequencies $\omega_{\rm TO}^{\parallel}$, $\omega_{\rm LO}^{\parallel}$, $\omega_{\rm TO}^{\perp}$, and $\omega_{\rm LO}^{\perp}$ of hBN (bottom to top). Red curves mark the zeros of Re $\epsilon_{\rm RPA}$. The dashed black lines show the line $y = x$ and mark the region where Im$\chi = 0$. The hybridization between phonon and plasmon modes is clear.

theory is of second order in the dressed interlayer interaction.[4,5] In terms of the variables carrier density, layer separation, and temperature, and under the assumptions that both layers are with high electron doping and $T \ll T_F$,[47] it reads (refer to Refs. 6 and 10 for details)

$$\rho_D = -\frac{\hbar}{e^2}\frac{\alpha_g^2}{8}\frac{\hbar v_F\sqrt{\pi n}}{k_B T}\int_0^\infty dx\int_0^\infty dy\, \mathcal{K}(T,d,n), \qquad (7)$$

where $\alpha_g = e^2/(4\pi\epsilon_{\rm vac}v_F\hbar)$ denotes the effective fine structure constant in graphene and the integral kernel

$$\mathcal{K} = \frac{k_F^2\epsilon_{\rm vac}^2}{e^4}\frac{|U_{12}(x,y)|^2}{\sinh^2\left(y\frac{T_F}{2T}\right)}\frac{x^7\,\Phi^2(x,y)}{x^2-y^2}. \qquad (8)$$

The function Φ, defined in Eq. (B1), is related to the nonlinear susceptibility of graphene, and restricts the integration range in the x,y plane to the region $\omega < v_F q$.

In order to estimate the contribution of phonon exchange to the drag effect, we note that the drag resistivity $\rho_{\rm CD}$ resulting from Coulomb interaction only (which is usually taken as a measure for Coulomb drag) is obtained by substituting the static value of the electron–electron interaction into the integral kernel Eq. (8):

$$\rho_{\rm CD} = \rho_D|_{U^{(0)}_{\lambda\lambda'}(q,\omega=0)}. \qquad (9)$$

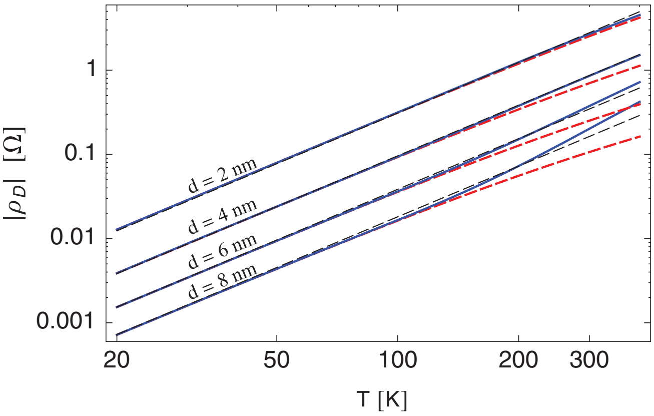

FIG. 3. (Color online) Drag resistivity versus temperature for various interlayer distances, $n = 0.02$ nm^{-2}. The blue curves show $|\rho_{\rm D}|$ [Eq. (7)] including interaction via phonon exchange and Coulomb interaction, the dashed red curves show $|\rho_{\rm CD}|$ [Eq. (9)] with Coulomb interaction only, and dashed black lines the low-temperature asymptote $\rho_{\rm CD}^{\rm low\,T}$ [Eq. (B2)]. The lowest pair of curves ($d = 8$ nm) is also plotted on a linear scale in Fig. 7.

For low temperatures $E_F \gg k_{\rm B}T$, the resistivity $\rho_{\rm CD}$ can be approximated by $\rho_{\rm CD}^{\rm low\,T} \propto T^2$ of Eq. (B2) (see Ref. 6 for a detailed derivation), under the additional condition $k_F d, k_F d/\epsilon_\parallel \gg 1$ (large layer spacing), this can be further approximated to yield[6]

$$\rho_{\rm CD}^{\rm large\ d} = -\frac{\hbar}{e^2}\frac{(\epsilon_0^\parallel)^3}{\epsilon_0^\perp}\frac{\zeta(3)}{\pi 2^8\alpha_g^2}\frac{(k_BT)^2}{(\hbar v_F)^2 n^3 d^4}. \qquad (10)$$

(Note that in the static limit, one only needs to rescale $d \to d\sqrt{\epsilon_\perp/\epsilon_\parallel}$ and $\alpha_g \to \alpha_g/\sqrt{\epsilon_\perp\epsilon_\parallel}$ to take into account the anisotropy of hBN.) The full blue curves in Figs. 3–5 show the absolute value of ρ_D Eq. (7) for different parameters T, n, and d, while $|\rho_{\rm CD}|$ is shown by dashed red curves, $\rho_{\rm CD}^{\rm low\,T}$ by the dashed black lines in Figs. 3 and 5, and the dotted green line in Fig. 5 shows $\rho_{\rm CD}^{\rm large\ d}$.

As Figs. 3 and 4 show, the contribution of phonon mediated interaction to the drag resistivity is vanishingly small at low temperatures, but becomes noticeable for $T > 150$ K, the effect being more pronounced the larger the layer separation. This temperature dependence is due to the factor $\sinh^{-2}[yT_F/(2T)]$ in the integration kernel Eq. (8), which suppresses the integrand for values of $y > T/T_F$. Thus at low temperatures the main contribution to the y integration in Eq. (7) comes from a frequency range where the dielectric

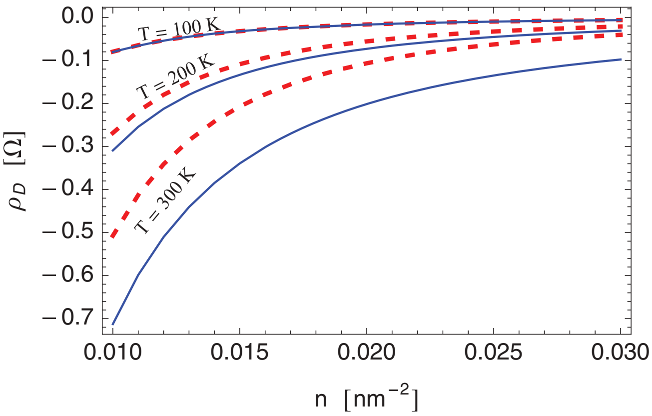

FIG. 4. (Color online) Drag resistivity versus carrier density for various temperatures $d = 8$ nm. Colors as in Fig. 3.

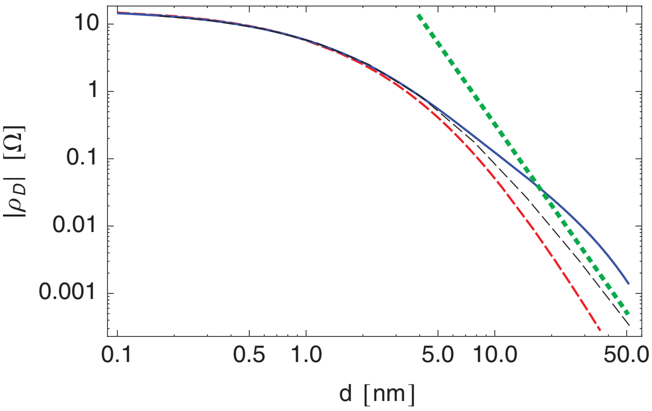

FIG. 5. (Color online) Drag resistivity versus layer separation for $T = 300$ K, $n = 0.02$ nm^{-2}. Colors as in Fig. 3. The low-temperature asymptote $\rho_{\rm CD}^{\rm low\,T}$ [dashed black curve, Eq. (B2)], converges for large layer separation to $\rho_{\rm CD}^{\rm large\,d}$ [dotted green line, Eq. (10)]. Note that at this temperature and density $\rho_{\rm CD}^{\rm low\,T}$ already differs from the full static calculation $\rho_{\rm CD}$.

functions in the integrand are still close to their static values. However, the phonon contribution becomes noticeable at lower temperatures than one would expect, taking into account that the energy of the lowest phonon mode $\hbar\omega_{\rm TO}^{\parallel}/k_B \approx 1100$ K. It is also interesting to notice that in the range from 100 to 250 K, the drag resistivity ρ_D, including the effect of phonons, is closer to the T^2 behavior $\rho_{\rm CD}^{\rm low\,T}$ than the purely Coulomb drag result $\rho_{\rm CD}$. The plot of $\mathcal{K}$ as a function of y in Fig. 6 shows the origin of the phonon contribution to the integral ρ_D: With rising temperature, peaks near the resonance frequencies $\omega_{\rm TO}^{\parallel}$ and $\omega_{\rm TO}^{\perp}$ appear in the integrand, which enhance the magnitude of ρ_D.

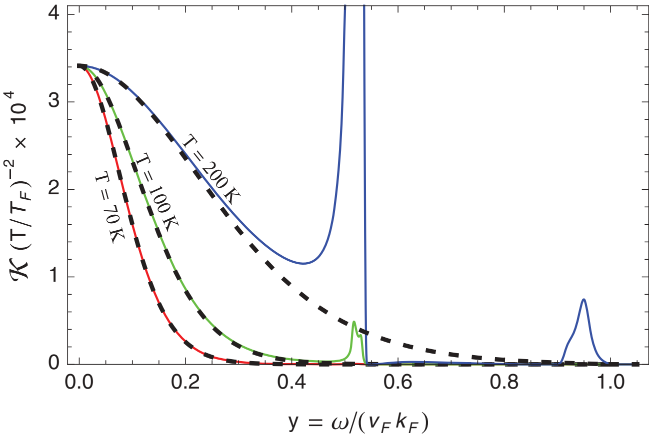

FIG. 6. (Color online) The integral kernel $\mathcal{K}$ of Eq. (8) with $x = q/k_F = 1$, $d = 8$ nm, $n = 0.02$ nm^{-2} as a function of $y = \omega/v_F k_F$ for the temperatures 200, 100, 70 K (full curves, from top to bottom). The curves have been aligned on the left side by dividing with the $y \to 0$ temperature dependence $(T/T_{\rm F})^2$. At $T = 100$ K (green curve) a peak near the resonance frequency $\omega_{\rm TO}^{\parallel}$ appears, at $T = 200$ K (blue curve) there is and additional second peak near $\omega_{\rm TO}^{\perp}$ (see the vertical green lines in Fig. 2). Dashed curves show the integral kernel for $\rho_{\rm CD}$, where these peaks are absent.

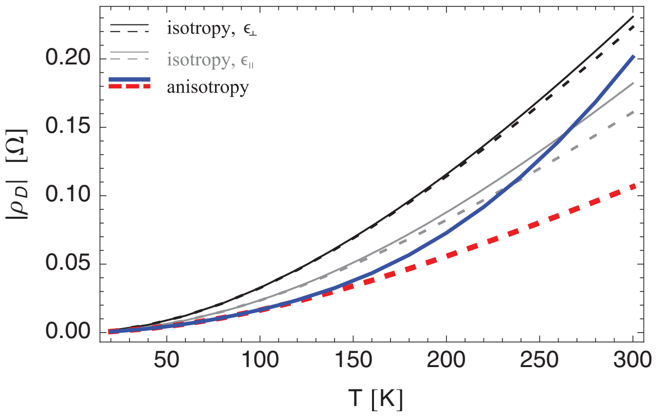

FIG. 7. (Color online) Effect of the anisotropy of hBN on the behavior of drag with temperature, with $n = 0.02$ nm^{-2} and $d = 8$ nm. The curves *isotropy*, $\epsilon_\parallel$ and *isotropy*, $\epsilon_\perp$ were computed assuming that the graphene layers are immersed in an isotropic dielectric medium, with dielectric functions given by $\epsilon_\parallel$ and $\epsilon_\perp$, respectively [see Eq. (2)]. The curve *anisotropy* was computed taking into account the anisotropy of hBN as in Eq. (4). Solid curves show $\rho_{\rm D}$, dashed ones $\rho_{\rm CD}$.

Figure 4 shows that the relative effect of phonon exchange on ρ_D is larger for high densities. For high values of n, the argument of the dielectric functions $\epsilon(\omega) = \epsilon(y v_F \sqrt{\pi n})$ in Eq. (8) reaches the resonance frequency already at lower values of y. While $\rho_{\rm CD}$ decreases rapidly with n due to increased screening of the Coulomb interaction, the modification of the screening function $\epsilon_{\rm RPA}$ by phonon interaction is seen to counteract this decrease at high temperatures.

Finally, Fig. 7 illustrates the effect of the anisotropy in hBN that enters ρ_D through the electron-electron interaction Eq. (4). We compare the drag resistivity in hBN with that in an isotropic medium with dielectric functions $\epsilon_\parallel$ and $\epsilon_\perp$, respectively [see Eq. (2)]. The difference in magnitude between ρ_D and $\rho_{\rm CD}$ is seen to be greatest in the anisotropic case, where both in-plane and out-of-plane phonon modes contribute to the interlayer interaction.

IV. SUMMARY AND DISCUSSION

We showed that including the electron–electron interaction via phonon exchange into the theory of Coulomb drag significantly changes the magnitude of the predicted drag resistivity in graphene-hBN heterostructures. For large layer separations, the deviations become noticeable at temperatures higher than 150 K.

As the lowest phonon resonance frequency in the spacer material hBN corresponds to a temperature of approximately 1100 K, our result at first sight seems to be at odds with the notion that phonon effects should be proportional to the thermal population factor of the relevant modes. This is indeed the case for other transport phenomena, like the substrate limited electron mobility in graphene, where real momentum transfer from an electronic state (in graphene) to a phonon mode (in a dielectric substrate material) plays a role.[24,38] The decay rate of the electronic state is then overall proportional to the thermal population of the phonon mode. Our scenario however involves the exchange of virtual phonons in a process that is of second order in the interlayer interaction,[5] and no decay processes into real phonon states are relevant for ρ_D. We note that in Ref. 7 the effect of substrate phonons on Coulomb drag was considered for the case where a material described by a uniform dielectric function fills what is our region III of Fig. 1, and a deviation from the low-temperature T^2 behavior of ρ_D was predicted for temperatures roughly an order of magnitude lower than the phononic resonance frequency of the substrate material.

Up to date, there remains considerable discrepancy between experimental data on Coulomb drag between graphene layers embedded in SiO$_2$/Al$_2$O$_3$[18,19] and hBN[20] and the existing theoretical work. For hBN, the reported drag resistivities in the Fermi liquid regime are roughly a factor of 3 larger than predicted, and the results of the present paper do not change this situation. The experimentally reported T^2 dependence of ρ_D for $d = 6$ nm and $n = 0.018$ nm^{-2} up to temperatures of 240 K[48] does not disagree with our results presented in Fig. 3. Actually, it appears that in the temperature range of 100 to 250 K the inclusion of phonon mediated interaction brings the behavior of drag closer to the low temperature T^2 behavior than with static Coulomb interaction only. Nevertheless, an extension of the experimental data shown in Ref. 20 up to room temperature would be needed to distinguish clearly between ρ_D and $\rho_{\rm CD}$. The use of other substrate materials, such as SiO$_2$, should not qualitatively alter the results of this paper. We think that future experiments with devices as considered in the present work will be able to check our predictions.

ACKNOWLEDGMENTS

The authors would like to thank N. M. R. Peres for useful discussions. Financial support from Fundação para a Ciência e a Tecnologia (Portugal) through Grant No. SFRH/BD/78987/2011 (B.A.), the Marie Curie ITN *NanoCTM* (J.S.), and from MICINN (Spain) through Grants No. FIS2010-21372 (F.S.) and No. FIS2008-00124 (F.G.) is acknowledged.

APPENDIX A : FRÖHLICH ELECTRON–PHONON COUPLING AND PHONON MEDIATED ELECTRON–ELECTRON INTERACTION

Throughout the present work we assume the dielectric properties of hBN layers forming heterostructures as shown in Fig. 1 to be the same as for bulk hBN.

The Fröhlich Hamiltonian describing the coupling of electrons to a bulk polar longitudinal phonon mode (in an isotropic homogeneous dielectric material) is given by[35–37]

$$H_{\text{e-ph}} = \int d^3r\rho(\mathbf{r})\frac{1}{\sqrt{V}}\sum_{\mathbf{Q}} M(Q)e^{i\mathbf{Q}\cdot\mathbf{r}}\left(a_{\mathbf{Q}} - a^\dagger_{-\mathbf{Q}}\right),$$

where $\rho(\mathbf{r})$ denotes the electron density operator, $a^\dagger_{\mathbf{Q}}$ ($a_{\mathbf{Q}}$) is the creation (annihilation) phonon operator with momentum $\mathbf{Q} = (q_x,q_y,q_z)$, and the matrix element reads

$$M(Q) = i\sqrt{\frac{e^2\omega_{\rm LO}}{2\epsilon_{\rm vac}Q^2}\left(\frac{1}{\epsilon_\infty} - \frac{1}{\epsilon_0}\right)}, \tag{A1}$$

with the longitudinal optical phonon frequency $\omega_{\rm LO}$. The phonon mediated interaction between electrons is given by

$$\psi(Q,\omega) = M(Q)M(Q)^* D_{\rm LO}(Q,\omega), \tag{A2}$$

with the bare phonon propagator

$$D_{\rm LO}(Q,\omega) = 2\omega_{\rm LO}/\left(\omega^2 - \omega_{\rm LO}^2\right). \tag{A3}$$

We employ the usual approximation of dispersionless optical phonons.[29,33,35,43]

The bare Coulomb interaction is given by

$$V_{\rm C} = e^2/(\epsilon_{\rm vac}\epsilon_\infty Q^2), \tag{A4}$$

where ϵ_∞ takes into account the high frequency screening properties of the medium.

With Eqs. (A2)–(A4) and the Lyddane-Sachs-Teller relation[46] $\omega_{\rm LO}^2/\omega_{\rm TO}^2 = \epsilon_0/\epsilon_\infty$, we arrive at the combined Coulomb and phonon mediated interaction

$$U(Q,\omega) = V_{\rm C}(Q) + \psi(Q,\omega) = \frac{e^2}{\epsilon_{\rm vac}\epsilon(\omega)Q^2}, \tag{A5}$$

with $\epsilon(\omega)$ the dielectric function of the medium, see Eq. (3). Since the Fröhlich coupling is derived in a phenomenological approach based on the dielectric properties of the material, the combined Coulomb and phonon mediated interaction simply reduces to the Coulomb interaction screened by $\epsilon(\omega)$, as it should.

In a two-layer system as shown in Fig. 1, the Fröhlich coupling coupling between bulk phonons and 2D electrons of layer λ is given by[43]

$$M_\lambda(q,q_z) = i\sqrt{\frac{e^2\omega_{\rm LO}}{2\epsilon_{\rm vac}\left(q^2+q_z^2\right)}\left(\frac{1}{\epsilon_\infty} - \frac{1}{\epsilon_0}\right)}e^{iq_z d(1-\delta_{\lambda 1})}, \tag{A6}$$

where $\mathbf{q} = (q_x,q_y)$ is a two-dimensional momentum vector. In analogy to the above, we now get for the combined Coulomb–phonon interaction in a homogeneous isotropic medium

$$\begin{aligned} U^{\rm iso}_{\lambda\lambda'}(q,\omega) &\equiv V_{\lambda\lambda'}(q) + \psi_{\lambda\lambda'}(q,\omega) \\ &= \frac{1}{\epsilon(\omega)}\frac{e^2}{2\epsilon_{\rm vac}q}e^{-qd(1-\delta_{\lambda\lambda'})}. \end{aligned} \tag{A7}$$

Although it is possible to generalize the Fröhlich electron–phonon coupling for the case of anisotropic materials[41,49] and inhomogeneous layered materials,[50] the easiest way to obtain the effective electron–electron interaction, taking into account the phonon mediated interaction, is by solving Poisson's equation for the electric potential created by a point charge in the dielectric medium taking into account the frequency dependence of its dielectric tensor.

APPENDIX B: MATHEMATICAL DETAILS

The dressed interlayer interaction Eq. (5) is the solution of the coupled set of Dyson equations

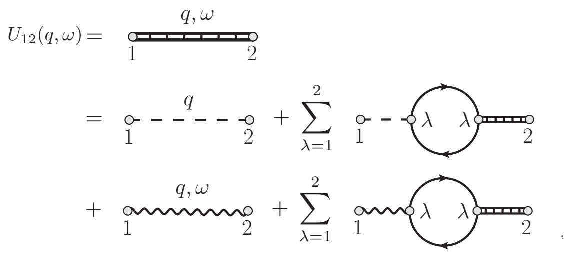

where the dashed and wiggled lines denote the bare Coulomb and phonon interaction, respectively, and the full curves electron propagators (see Refs. 5 and 31).

The function $\Phi(x,y)$ appearing in Eq. (8) reads[6,10]

$$\Phi(x,y) = \Phi^{+}(x,y)\,\Theta(y-x+2)\Theta(x-y) + \Phi^{-}(x,y)\,\Theta(1-y-|1-x|), \qquad \text{(B1)}$$

where

$$\Phi^{\pm} = \pm\cosh^{-1}\left(\frac{2\pm x}{y}\right) \mp \frac{2\pm x}{y}\sqrt{\left(\frac{2\pm x}{y}\right)^{2}-1}.$$

For the low-temperature approximation of ρ_D, the factor $\sinh^{-2}[yT_F/(2T)]$ in the integration kernel Eq. (8), which suppresses the integrand for values of $y > T/T_F$, allows one to expand the remaining integrand to the lowest order of y. The y integration can then be performed, yielding

$$\rho_{\mathrm{CD}}^{\mathrm{low\,T}} = -\frac{\hbar}{e^{2}}\frac{2\pi\alpha_{\mathrm{eff}}^{2}(k_BT)^{2}}{3n(\hbar v_F)^{2}}\int_0^2 dx\,\left\{e^{-2dx\sqrt{\pi n\epsilon_0^{\perp}/\epsilon_0^{\parallel}}} \times \frac{x^{3}(4-x^{2})}{\left[(x+4\alpha_{\mathrm{eff}})^{2}-16\alpha_{\mathrm{eff}}^{2}\exp(-2dx\sqrt{\pi n\epsilon_0^{\perp}/\epsilon_0^{\parallel}})\right]^{2}}\right\}, \qquad \text{(B2)}$$

where $\alpha_{\mathrm{eff}} \equiv \alpha_g/\sqrt{\epsilon_0^{\perp}\epsilon_0^{\parallel}}$ (see Ref. 6 for details).

---

[1] T. J. Gramila, J. P. Eisenstein, A. H. MacDonald, L. N. Pfeiffer, and K. W. West, Phys. Rev. Lett. **66**, 1216 (1991).

[2] U. Sivan, P. M. Solomon, and H. Shtrikman, Phys. Rev. Lett. **68**, 1196 (1992).

[3] L. Zheng and A. H. MacDonald, Phys. Rev. B **48**, 8203 (1993).

[4] K. Flensberg, B. Y.-K. Hu, A.-P. Jauho, and J. M. Kinaret, Phys. Rev. B **52**, 14761 (1995).

[5] A. Kamenev and Y. Oreg, Phys. Rev. B **52**, 7516 (1995).

[6] B. Amorim and N. M. R. Peres, J. Phys.: Condens. Matter **24**, 335602 (2012).

[7] M. Carrega, T. Tudorovskiy, A. Principi, M. I. Katsnelson, and M. Polini, New J. Phys. **14**, 063033 (2012).

[8] M. I. Katsnelson, Phys. Rev. B **84**, 041407 (2011).

[9] B. N. Narozhny, M. Titov, I. V. Gornyi, and P. M. Ostrovsky, Phys. Rev. B **85**, 195421 (2012).

[10] N. M. R. Peres, J. M. B. L. dos Santos, and A. H. C. Neto, Europhys. Lett. **95**, 18001 (2011).

[11] E. H. Hwang, R. Sensarma, and S. Das Sarma, Phys. Rev. B **84**, 245441 (2011).

[12] W.-K. Tse, B. Y.-K. Hu, and S. Das Sarma, Phys. Rev. B **76**, 081401 (2007).

[13] S. M. Badalyan and F. M. Peeters, Phys. Rev. B **86**, 121405(R) (2012).

[14] B. Scharf and A. Matos-Abiague, Phys. Rev. B **86**, 115425 (2012).

[15] M. Schütt, P. M. Ostrovsky, M. Titov, I. V. Gornyi, B. N. Narozhny, and A. D. Mirlin, arXiv:1205.5018.

[16] J. C. W. Song and L. S. Levitov, arXiv:1205.5257.

[17] A. H. Castro Neto, F. Guinea, N. M. R. Peres, K. S. Novoselov, and A. K. Geim, Rev. Mod. Phys. **81**, 109 (2009).

[18] S. Kim, I. Jo, J. Nah, Z. Yao, S. K. Banerjee, and E. Tutuc, Phys. Rev. B **83**, 161401 (2011).

[19] S. Kim and E. Tutuc, Solid State Commun. **152**, 1283 (2012).

[20] R. V. Gorbachev, A. K. Geim, M. I. Katsnelson, K. S. Novoselov, T. Tudorovskiy, I. V. Grigorieva, A. H. MacDonald, K. Watanabe, T. Taniguchi, and L. A. Ponomarenko, arXiv:1206.6626.

[21] A.-P. Jauho and H. Smith, Phys. Rev. B **47**, 4420 (1993).

[22] R. C. Dean, A. F. Young, I. Meric, C. Lee, L. Wang, S. Sorgenfrei, K. Watanabe, T. Taniguchi, P. Kim, K. L. Shepard *et al.*, Nat Nano **5**, 722 (2010).

[23] A. S. Mayorov, R. V. Gorbachev, S. V. Morozov, L. Britnell, R. Jalil, L. A. Ponomarenko, P. Blake, K. S. Novoselov, K. Watanabe, T. Taniguchi *et al.*, Nano Lett. **11**, 2396 (2011).

[24] J. Schiefele, F. Sols, and F. Guinea, Phys. Rev. B **85**, 195420 (2012).

[25] J. M. Garcia, U. Wurstbauer, A. Levy, L. N. Pfeiffer, A. Pinczuk, A. S. Plaut, L. Wang, C. R. Dean, R. Buizza, A. V. D. Zande *et al.*, Solid State Commun. **152**, 975 (2012).

[26] L. A. Ponomarenko, A. K. Geim, A. A. Zhukov, R. Jalil, S. V. Morozov, K. S. Novoselov, I. V. Grigorieva, E. H. Hill, V. V. Cheianov, V. I. Fal'ko *et al.*, Nat. Phys. **7**, 958 (2011).

[27] L. Britnell, R. V. Gorbachev, R. Jalil, B. D. Belle, F. Schedin, A. Mishchenko, T. Georgiou, M. I. Katsnelson, L. Eaves, S. V. Morozov *et al.*, Science **335**, 947 (2012).

[28] L. Britnell, R. V. Gorbachev, R. Jalil, B. D. Belle, F. Schedin, M. I. Katsnelson, L. Eaves, S. V. Morozov, A. S. Mayorov, N. M. R. Peres *et al.*, Nano Lett. **12**, 1707 (2012).

[29] R. Jalabert and S. Das Sarma, Phys. Rev. B **40**, 9723 (1989).

[30] H. C. Tso, P. Vasilopoulos, and F. M. Peeters, Phys. Rev. Lett. **68**, 2516 (1992).

[31] C. Zhang and Y. Takahashi, J. Phys.: Condens. Matter **5**, 5009 (1993).

[32] T. J. Gramila, J. P. Eisenstein, A. H. MacDonald, L. N. Pfeiffer, and K. W. West, Phys. Rev. B **47**, 12957 (1993).

[33] K. Güven and B. Tanatar, Phys. Rev. B **56**, 7535 (1997).

[34] M. C. Bønsager, K. Flensberg, B. Y.-K. Hu, and A. H. MacDonald, Phys. Rev. B **57**, 7085 (1998).

[35] H. Fröhlich, Adv. Phys. **3**, 325 (1954).

[36] G. D. Mahan, *Many-Particle Physics* (Plenum, New York, 1981).

[37] M. P. Marder, *Condensed Matter Physics*, 2nd ed. (John Wiley, Hoboken, NJ, 2010).

[38] S. Fratini and F. Guinea, Phys. Rev. B **77**, 195415 (2008).

[39] J.-H. Chen, C. Jang, S. Xiao, M. Ishigami, and M. S. Fuhrer, Nat. Nanotechnol. **3**, 206 (2008).

[40] See Refs. 44,51, and 52 for details on the phonon dispersions of hBN, and the classification of the vibrational modes into Raman active, infrared active, and optically silent. Figure 3 and Eqs. 21 and 24 of Ref. 51 show how the long range Coulomb potential associated with the infrared active modes leads to the splitting of transverse and longitudinal optical frequencies at the Γ point.

[41] R. Loudon, Adv. Phys. **13**, 423 (1964).

[42] We are here using the retarded expression (defined as being analytic in the upper half of the complex ω plane) in order to be consistent with the likewise retarded polarizability of graphene taken from Ref. 53. Not keeping this consistency yields significantly different results.

[43] S. Sarma and B. Mason, Ann. Phys. **163**, 78 (1985).

[44] R. Geick, C. H. Perry, and G. Rupprecht, Phys. Rev. **146**, 543 (1966).

[45] In the numerical calculations we use for simplicity the zero temperature expression for χ as calculated in Refs. 53 and 54, which is a good approximation for $T \ll T_F$, with T_F the Fermi temperature.

[46] R. H. Lyddane, R. G. Sachs, and E. Teller, Phys. Rev. **59**, 673 (1941).

[47] We here use a simplified form of the nonlinear susceptibility of graphene, which is valid for electron doping high enough such that the existence of the valence band can be ignored. The condition $T \ll T_F$ is important as we use the zero temperature expressions for the polarizability of graphene. See Refs. 6 and 10 for a discussion of both approximations.

[48] See Fig. 2(a) in Ref. 20.

[49] M. A. Stroscio and M. Dutta, *Phonons in Nanostructures* (Cambridge University Press, Cambridge, 2003).

[50] N. Mori and T. Ando, Phys. Rev. B **40**, 6175 (1989).

[51] K. H. Michel and B. Verberck, Phys. Rev. B **83**, 115328 (2011).

[52] J. Serrano, A. Bosak, R. Arenal, M. Krisch, K. Watanabe, T. Taniguchi, H. Kanda, A. Rubio, and L. Wirtz, Phys. Rev. Lett. **98**, 095503 (2007).

[53] B. Wunsch, T. Stauber, F. Sols, and F. Guinea, New J. Phys. **8**, 318 (2006).

[54] E. H. Hwang and S. Das Sarma, Phys. Rev. B **75**, 205418 (2007).